Scientific Reports

https://doi.org/10.1038/s41598-026-36660-6

Article in Press

Numerical modeling of coupled stress-fracture evolution in water-resisting key strata during longwall mining

Received: 16 July 2025

Accepted: 14 January 2026

Published online: 29 January 2026

Cite this article as: Gao H., Ji L., Huang Y. *et al.* Numerical modeling of coupled stress-fracture evolution in water-resisting key strata during longwall mining. *Sci Rep* (2026). https://doi.org/10.1038/s41598-026-36660-6

Huadong Gao, Li Ji, Yanli Huang & Junmeng Li

Numerical Modeling of Coupled Stress-Fracture Evolution in Water-Resisting Key Strata During Longwall Mining

Huadong Gao[1], Li Ji[2,*], Yanli Huang[3], Junmeng Li[3]

[1] College of Architecture and Energy Engineering, Wenzhou University of Technology, Wenzhou 325027, China;

[2] School of Economics and Management, Wenzhou University of Technology, Wenzhou 325027, China;

[3] School of Mines, China University of Mining and Technology, Xuzhou 221116, China

* Corresponding author. E-mail address: jessie201708@163.com (L. Ji)

Abstract: During underground coal mining, the evolution of stress and fracture development within the overlying water-resisting key strata (WRKS) significantly impacts its water-resisting properties, thereby making it a critical factor controlling the stability of groundwater seepage in coal mines. Utilizing UDEC and based on the coal-rock interburden thickness, the development height of the water-conducting fracture zone, and the theory of the “three mining-induced zones” (caved zone, fractured zone, continuous deformation zone), numerical models simulating coal seam excavation and the response of the WRKS under various relative interburden thickness conditions were constructed. These models were employed to investigate the mining-induced stress paths and fracture evolution characteristics of the WRKS at different spatial positions during coal seam advance. The results demonstrate that: The characteristic spatial distribution pattern of mining-induced stress within the WRKS follows the sequence “Initial Stress Zone - Stress Concentration Zone - Pressure Relief Zone - Stress Recovery Zone - Pressure Relief Zone - Stress Concentration Zone - Initial Stress Zone”. The maximum stress concentration factor within the stress concentration zone exhibits a negative correlation with the relative interburden thickness, while the minimum stress concentration factor within the pressure relief zone shows a positive correlation with the relative interburden thickness. The spatial extent of the

fracture development zone within the WRKS exhibits a high degree of coincidence with the pressure relief zone; furthermore, the extent, duration, and fracture density of the fracture development zone all exhibit negative correlations with the relative interburden thickness. The mining-induced stress path experienced by the WRKS comprises six distinct stages: “Original Rock Stress - Stress Increase - Pressure Relief - Stabilized Pressure Relief - Stress Recovery - Asymptotically Approaching Original Rock Stress”. Concurrently, the evolution process of mining-induced fractures progresses through five stages: “Incubation - Expansion - Stabilization - Closure - Asymptotically Approaching Complete Closure”.

Key words: water-resisting key stratum; mining-induced stress path; mining-induced fracture evolution; numerical simulation; water-preserved coal mining

1 Introduction

Research on water-preserved coal mining serves as the theoretical foundation for both water resource protection and high-quality coal development in the ecologically fragile mining areas of Northwest China[1-4]. Within the framework of water-preserved coal mining, protecting the integrity of the WRKS is a primary objective for preventing water inrush disasters in coal mines and safeguarding water resources[5-7]. The WRKS, located within the overlying strata of the coal seam, plays a crucial role in controlling the stability of groundwater seepage[8,9]. During the mining process, the characteristics of its stress evolution and fracture development significantly impact its water-resisting properties[10].

Prior to coal mining activities, overlying strata exist in a state of virgin rock stress. Coal extraction disrupts this stress equilibrium, subjecting the strata to mining-induced stress changes that ultimately drives deformation and failure[11-13]. In the study of mining-induced stress changes caused by coal seam extraction, scholars have achieved significant research outcomes. Through physical simulation, Deng et al.[14] revealed a four-stage evolutionary pattern of mining-induced stress: gentle stability, gradual accumulation,

high-level mutation, and return to stability. Huang et al.[15] concluded that during the mining of coal seams in multi-seam conditions, the lower working face undergoes three distinct stages: mining compression, pressure relief expansion, and stress recovery. Xie et al.[16] proposed a four-stage model simulating the unloading expansion stress evolution process in protected seams during protective layer mining, consisting of geostress recovery, axial compression, pressure relief expansion, and stress recovery. Through numerical simulations, Cui et al.[17] revealed that vertical stress during working face advancement progresses through three phases: initial geostress, periodic fluctuation with stepwise increase, and abrupt decrease. Gao et al.[18] identified in-situ mining disturbance stress paths through field tests, demonstrating that axial stress evolves from initial state to peak stress during face advancement, followed by reduction to residual strength with rock failure, while lateral pressure continuously unloads from initial state to lower levels. Zhang et al.[19] summarized the stress path evolution in protected seams under repeated mining activities into three phases: loading, unloading, and recovery. Ma et al.[20] established a mechanical model for the fracture of water-resisting key stratum in multi-seam mining and validated its effectiveness in water inrush risk assessment through numerical simulation and field microseismic monitoring. Chai et al.[21] discovered that floor rock stress distribution during upper protective layer mining can be divided into four phases along the advancing direction: original rock stress, stress concentration, stress release, and stress recovery. Xie et al.[22] employed numerical simulation methods to investigate the characteristics of stress changes within the overlying strata during mining, specifically considering variations in the interburden thickness between the overlying strata and the coal seam. Pang et al.[23] studied the spatiotemporal evolution characteristics of mining-induced stress in the overlying strata above deep mining faces and the associated fracturing and instability processes.

In research concerning the evolution characteristics of mining-

induced fractures within overlying strata, Wang et al.[24] conducted physical similarity simulation tests, quantitatively analyzing the power-law distribution characteristics of the fracture network from geometric and topological perspectives. Through similarity simulation experiments, Ran et al.[25] revealed the asymmetric evolution characteristics of mining-induced fractures under inclined multi-seam mining conditions. Zhao et al.[26] employed the method of physical similarity simulation for coal seam mining to study the development and spatial distribution patterns of fracture networks in roof strata under mining disturbance. Through combined numerical simulation of repeated mining and physical similarity simulation tests, Wu et al.[27] obtained the developmental characteristics and spatial distribution morphology of the overlying strata fracture network. Liang et al.[28] investigated the evolution laws of the mining-induced fracture network in overlying strata by performing physical similarity simulation tests on strata fracture and caving during coal seam extraction. Yin et al.[29] analyzed the geometric structural features and spatial distribution patterns of fractures within the overlying strata by conducting three-dimensional simulated mining experiments. Based on the quantification of mining-induced fracture dimensions in overlying strata, Zhang et al.[30] revealed the developmental characteristics of vertical fractures and the concentration patterns of specific fracture angles. Liu et al.[31] utilized fractal dimension to provide a quantitative description of the development laws of fractures within the overlying strata. Chen et al.[32] first performed UDEC numerical simulations of overlying strata movement induced by mining, obtaining the developmental morphology of the fracture network, and then quantitatively described its structural characteristics using fractal theory. Zhuo et al.[33] found significant differences in the fracture aperture evolution processes between the compacted zone in the middle of the goaf and the fracture development zones on both sides within the overlying strata during mining. Chen et al.[34] classified rock stratum fractures into shear fractures, bed-

separation fractures, and longitudinal tensile fractures, establishing the coupling relationship between fracture propagation in the roof and floor and stress under mining influence. Yao et al.[35] combined discrete element simulation with the transient electromagnetic method (TEM) to achieve mutual verification of mining-induced fracture distribution in overlying strata.

In summary, current research predominantly employs methods such as numerical simulation and field measurements to investigate the mining-induced mechanical behavior of coal and rock strata, utilizing physical similarity simulation tests to study the evolution laws of fractures within overlying strata, and applying fractal theory to quantitatively describe fracture development characteristics. However, studies focusing on the mining-induced stress paths and fracture evolution characteristics at different spatial positions within rock strata, along with the interrelationship between mining-induced stress evolution and fracture development, have received relatively limited attention. Building upon the simplification of treating rock strata as homogeneous structures, this study shifts its focus from examining the overall behavior or localized static states of the stratum to investigating a previously underexplored question: Throughout the mining process, how do different spatial locations within the same rock stratum undergo a complete and sequential dynamic evolution of stress and fracture? This internal spatial variation is critical for accurately determining both the global stability and local failure mechanisms of key strata.

To address these knowledge gaps, the authors have systematically investigated the mining-induced stress paths and fracture evolution characteristics of the WRKS at different spatial positions during coal seam advance. Utilizing UDEC, numerical models simulating coal seam excavation and WRKS response under various relative interburden thickness conditions were constructed. This approach reveals the distribution and variation patterns of mining-induced stress and fractures within the WRKS and explores the relationship between them. The core innovation of this study lies

in establishing a dynamic evolution sequence of stress-fracture in the WRKS above the working face, which systematically accounts for the influence of relative interburden thickness throughout the entire mining process.

2 Numerical model

2.1 Controlling effect of relative interburden thickness

Prior to coal seam extraction, the overlying strata exist in a state of true triaxial in-situ stress equilibrium[36]. Mining-induced excavation disturbance triggers redistribution of vertical and horizontal stresses within these strata, driving progressive upward deformation and failure that forms three distinct zones: the caved zone, fractured zone, and continuous deformation zone[37]. The vertical distance between individual strata and the coal seam governs their susceptibility to mining impacts, consequently generating variations in mining-induced stress paths and fracture evolution. The WRKS – defined as a competent stratum between the coal seam and overlying aquifer that controls rock mass deformation – functions independently or with low-permeability weak strata as a structural barrier resisting certain levels of stress and hydrostatic pressure[38]. Post-mining WRKS behavior fundamentally depends on its position within these zones: within the continuous deformation zone, minimal fractures develop while strata undergo gentle elastic subsidence with preserved permeability; within the fractured zone, extensive longitudinal/transverse fractures degrade water-resisting capacity despite retained stratification; within the caved zone, fragmentation into chaotic rock blocks enables unrestricted groundwater flow, resulting in complete hydraulic integrity loss[39-41].

The structural and seepage stability of the WRKS under coal seam excavation disturbance is fundamentally governed by the development height of the fractured zone and the interburden thickness. As summarized in Table 1, empirical formulas for predicting the development height of water-conducting fracture zones – documented in the Specification for Coal Pillar Retention and Pressure Mining beneath Structures, Water Bodies, Railways, and

Major Shafts and the Code for Hydrogeological and Engineering Geological Exploration in Mining Areas – demonstrate that this height primarily depends on mining height and overburden lithology[42,43]. Consequently, under specific geological conditions of a working face, the positioning of the WRKS within the fractured zone is predominantly controlled by the relative interburden thickness (ratio of interburden thickness to mining height). Larger relative interburden thickness corresponds to diminished excavation disturbance effects on the WRKS, thereby inducing systematic variations in its stress-fracture characteristics according to this geometric parameter.

Table 1 Empirical formulas for predicting the height of water-conducting fracture zones

Overburden lithology classification	Maximum development height of water-conducting fracture zones	
	Formula A	Formula B
Competent	$H_f = \frac{100\sum M}{1.2\sum M + 2.0} \pm 8.9$	$H_f = 30\sqrt{\sum M} + 10$
Medium-competent	$H_f = \frac{100\sum M}{1.6\sum M + 3.6} \pm 5.6$	$H_f = 20\sqrt{\sum M} + 10$
Incompetent	$H_f = \frac{100\sum M}{3.1\sum M + 5.0} \pm 4.0$	$H_f = 10\sqrt{\sum M} + 5$
Extremely incompetent	$H_f = \frac{100\sum M}{5.0\sum M + 8.0} \pm 3.0$	/

Note: $\sum M$ denotes cumulative mining height (m).

2.2 Geometric model construction

To investigate the mining-induced stress paths and fracture evolution characteristics of the WRKS under varying relative interburden thickness conditions, a numerical model was constructed using the discrete element software UDEC (Universal Distinct Element Code, version 7.0; https://www.itascacg.com/software/udec), as illustrated in Fig. 1. Crucially, this study focuses on elucidating fundamental principles

governing stress redistribution and fracture development in overlying strata during near-horizontal coal seam extraction, deliberately abstracted from site-specific geological constraints. The model disregards tectonic stresses within the mining zone and assumes a hydrostatic in-situ stress field where the rock mass experiences a triaxial compressive state with equal principal stress magnitudes[44,45]. This study employs a hydrostatic stress assumption to isolate the effect of relative interburden thickness from the confounding influence of tectonic stresses. This simplification is appropriate for fundamental investigation but requires modification with local in-situ stress field data for site-specific applications. As shown in Fig. 1, the geometric model spans 600 m (strike length) × 150 m (height), incorporating 100 m boundary coal pillars on both strike-direction flanks to simulate a 400 m effective mining advance. With wide boundary coal pillars on both flanks and a total advance distance that surpasses the critical threshold for a stable mining-induced stress field, the model minimizes boundary effects, thus ensuring that the results in the central analysis zone are representative. Through UDEC-simulated seam excavation and strata caving processes, we systematically analyze WRKS stress-fracture dynamics while quantifying the influence of relative interburden thickness on these mechanisms.

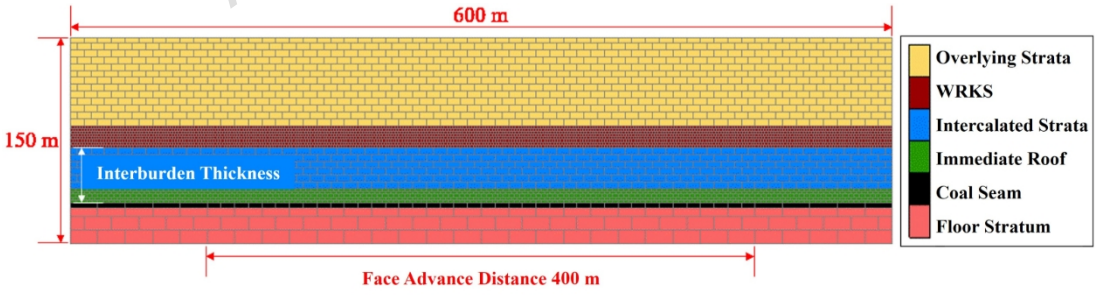

Fig. 1 Numerical geometric model

2.3 Simulation parameters configuration

The vertical distance between the WRKS and coal seam is defined as the interburden thickness. This geometric model maintains fixed parameters: 4 m mining height and medium-competent overburden lithology. Empirical formulas for water-

conducting fracture zones yield predicted heights of 34.4-50 m. To investigate WRKS stress-fracture dynamics under varying structural positions, three computational cases were designed with interburden thicknesses of 20, 40, and 60 m – corresponding to relative interburden thicknesses of 5, 10, and 15. These configurations intentionally position the WRKS within the caved zone, fractured zone, and continuous deformation zone, respectively. Boundary conditions include: fixed constraint at the model base; 11.55 MPa vertical stress applied at the top surface (simulating ~600 m burial depth); and gradient lateral stresses maintaining an isotropic lateral pressure coefficient (K=1) throughout the simulation. The simplified hydrostatic stress condition was adopted to decouple mining-induced stress perturbations from complex tectonic stresses. This approach enables a clearer focus on revealing the controlling effect of relative interburden thickness on WRKS behavior. The coal-rock mechanical parameters employed in this study (Table 2) are based on standardized laboratory tests on core samples from typical stratigraphic sequences in our research area, as established in[46]. The parameters are characterized by competent floor / intercalated / overlying strata mechanically contrasted with lower-strength coal seam, immediate roof, and WRKS[47]. The model simulates the advancement of the coal seam along the strike direction of the working face in increments of 10 m. This value was selected to balance computational efficiency with a spatial resolution sufficient to capture the evolution of stress and fracture fields. It should be noted that this increment controls the stepwise progression of the mining face in the model to achieve equilibrium at each step; it does not simulate the actual duration of excavation operations or time-dependent rock mass behaviors (e.g., creep). The primary focus of this study lies in the spatial progression of mining and the resulting equilibrium states.

Table 2 Mechanical parameters of coal and rock

Rock stratum	Thickness (m)	Density (kg·m^{-}	Bulk modulus	Shear modulus	Cohesion (MPa)	Tensile strength	Angle of intern

		^{3})	(GPa)	(GPa)		(MPa)	al frictio n (°)
Overlying strata	84/64/4 4	2500	10.0	7.3	2.3	1.4	35
WRKS	16	2200	7.3	3.8	1.5	1.27	28
Intercalat ed strata	10/30/5 0	2500	10.0	7.3	2.3	1.4	35
Immediat e roof	10	2200	7.3	3.8	1.5	1.27	28
Coal seam	4	1460	3.0	2.4	1.2	0.98	22
Floor strata	26	2500	10.0	7.3	2.3	1.4	35

3 Analysis of simulation results

3.1 Spatiotemporal evolution and variation patterns of mining-induced stresses in WRKS

Following computational equilibrium after each mining step, vertical and horizontal stress nephograms were exclusively extracted for the WRKS by hiding other strata layers. Fig. 2 visualizes the spatial distribution of WRKS stress fields at working face advance distances of 150, 200, 250, 300, 350, and 400 m under varying relative interburden thickness conditions.

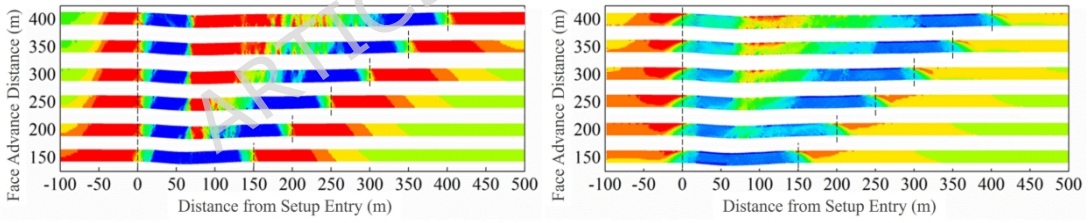

(a) Relative interburden thickness η=5

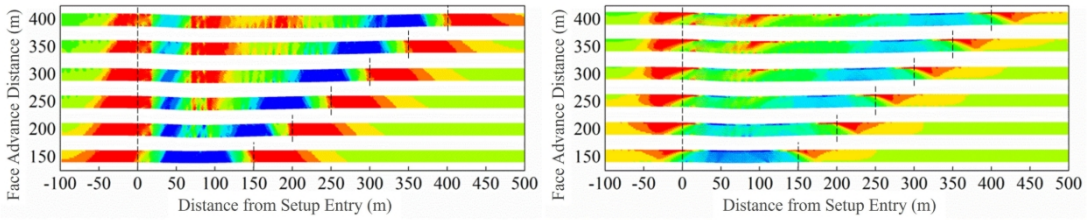

(b) Relative interburden thickness η=10

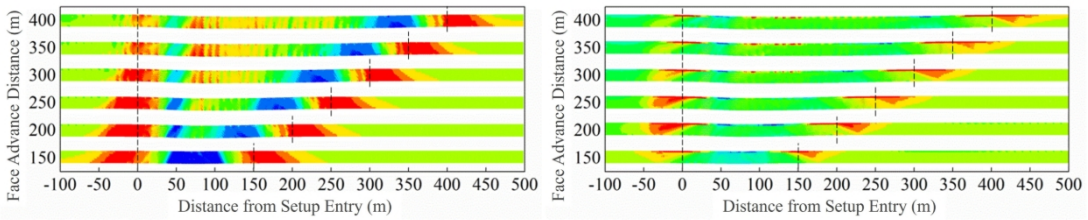

(c) Relative interburden thickness η=15

Fig.2 Spatial distribution of vertical and horizontal stresses in WRKS during mining

Analysis of Fig. 2(a) reveals the following stress evolution:

(1) At 150 m working face advance, vertical stress within the goaf area of the WRKS is significantly lower than in-situ stress, characterizing a pressure relief zone. Conversely, vertical stress exceeds in-situ levels within approximately 150 m behind the setup entry and ahead of the working face, defining stress concentration zones. This configuration establishes a sequential WRKS vertical stress distribution: Initial Stress Zone - Stress Concentration Zone - Pressure Relief Zone - Stress Concentration Zone - Initial Stress Zone. By 200 m advance, vertical stress begins to increase in the central relief zone, exhibiting localized stress concentrations. This phenomenon results from the WRKS bearing overburden loads, transforming the central relief area into a stress recovery zone. Consequently, the WRKS stress distribution pattern evolves to: Initial Stress Zone - Stress Concentration Zone - Pressure Relief Zone - Stress Recovery Zone - Pressure Relief Zone - Stress Concentration Zone - Initial Stress Zone. This configuration remains consistent thereafter, as validated in Fig. 3.

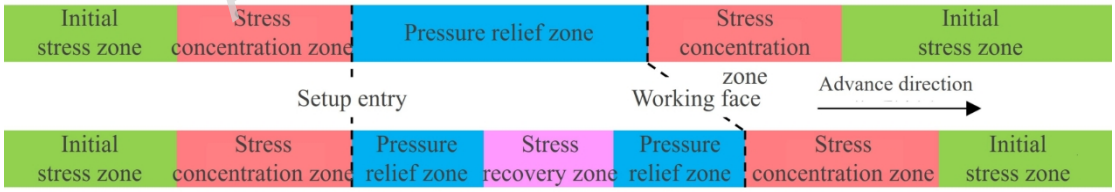

Fig. 3 Stress distribution patterns in WRKS pre- and post-stress rebalancing of mined-out areas

(2) As the working face advanced, the spatial extent of the stress recovery zone within the WRKS progressively expanded. Quantitative measurements recorded recovery zone widths of 0 m, 25 m, 60 m, 99 m, 145 m, and 193 m at working face advance distances of 150 m, 200 m, 250 m, 300 m, 350 m, and 400 m, respectively. Conversely, the stress concentration zone behind the setup entry exhibited progressive contraction, reducing to 60 m at

400 m advance – representing a 60% decrease compared to its initial extent at 150 m advance. The stress recovery zone and setup entry-side concentration zone collectively bore the overburden load from the panel's initial mining sector. The expanding recovery zone gradually became the primary load-bearing component, thereby driving the reduction of the concentration zone. Notably, the relief zone ahead of the setup entry maintained a virtually constant width of 59 m with fixed spatial positioning, while the relief zone behind the working face (122 m wide) and concentration zone ahead of the face (150 m wide) retained their dimensions but migrated synchronously with face advancement.

(3) The spatial distribution and evolutionary characteristics of vertical stress within the WRKS demonstrate mechanistic consistency at relative interburden thicknesses η=10 and 15 compared to η=5. At 250 m advance, quantitative measurements reveal progressive zonal contractions: the setup entry rear concentration zone decreases from 89 m (η=5) to 83 m (η=10) to 71 m (η=15); the setup entry front relief zone contracts from 59 m to 46 m to 43 m; the stress recovery zone diminishes from 60 m to 51 m to 35 m; the working face rear relief zone reduces from 122 m to 120 m to 115 m; and the working face front concentration zone narrows from 150 m to 126 m to 103 m. This systematic reduction across all zones (mean contraction rate: -11.2 m/η unit) stems from attenuated mining-induced disturbance effects on the WRKS at greater relative interburden thicknesses under identical geomechanical conditions. Horizontal stress evolution exhibits analogous spatiotemporal patterns.

A 600 m stress monitoring line was deployed along the base of the WRKS with 61 monitoring points spaced at 10 m intervals, tracking vertical and horizontal stress magnitudes at each point during coal seam extraction. Stress concentration coefficients across WRKS were plotted for advance distances of 150 m, 200 m, 250 m, 300 m, 350 m, and 400 m, as illustrated in Fig. 4.

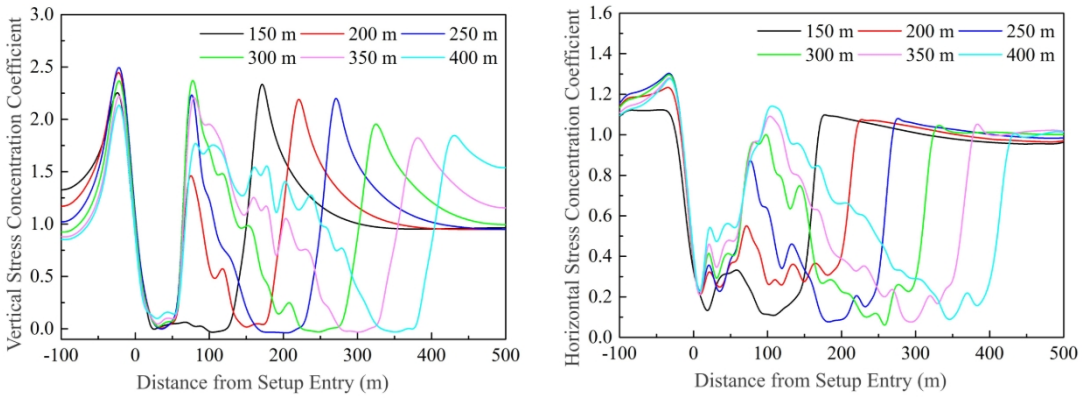

(a) Relative interburden thickness η=5

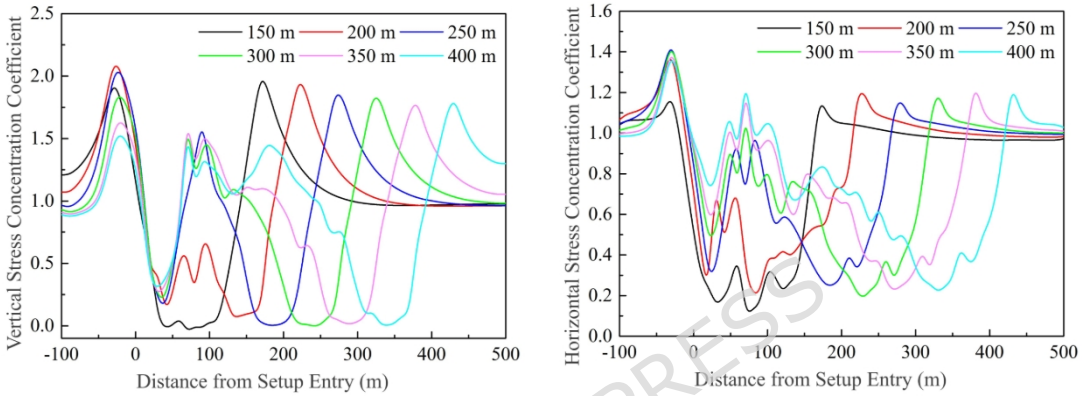

(b) Relative interburden thickness η=10

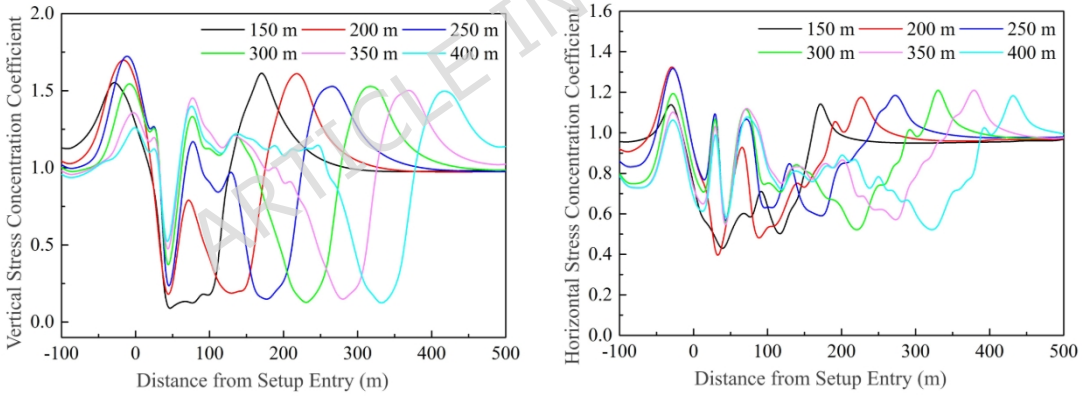

(c) Relative interburden thickness η=15

Fig. 4 Stress concentration coefficients for vertical and horizontal stresses in WRKS

Analysis of Fig. 4 demonstrates that:

(1) Relatively stable pressure relief and concentration zones persist ahead of and behind the setup entry throughout working face advancement. For relative interburden thicknesses η=5, 10, and 15, the mean maximum vertical stress concentration coefficients in the concentration zones progressively decrease from 2.45 to 1.87 and 1.54, while the mean minimum vertical stress concentration

coefficients in the relief zones correspondingly increase from 0.05 to 0.17 and 0.22.

(2) During coal seam advance, the stress concentration zone ahead of the working face and the relief zone behind it migrate synchronously forward while the stress recovery zone progressively expands. For relative interburden thicknesses η=5, 10, and 15, the variation amplitude (difference between maximum and minimum values) of vertical stress concentration coefficients in the WRKS decreases progressively from 2.57 to 2.11 and 1.62, indicating a systematic reduction in mining-induced disturbance intensity. This trend predicts that at sufficiently large η values, the WRKS would ultimately become entirely unaffected by mining activities, maintaining constant stress concentration coefficients of 1.0 (i.e., perpetual virgin stress state). Horizontal stress evolution exhibits analogous spatiotemporal patterns to vertical stress dynamics under identical conditions.

Six monitor points positioned 150 m, 200 m, 250 m, 300 m, 350 m, and 400 m ahead of the setup entry were selected to track vertical stress (syy) and horizontal stress (sxx) evolution during coal seam advance, with their variation curves plotted in Fig. 5.

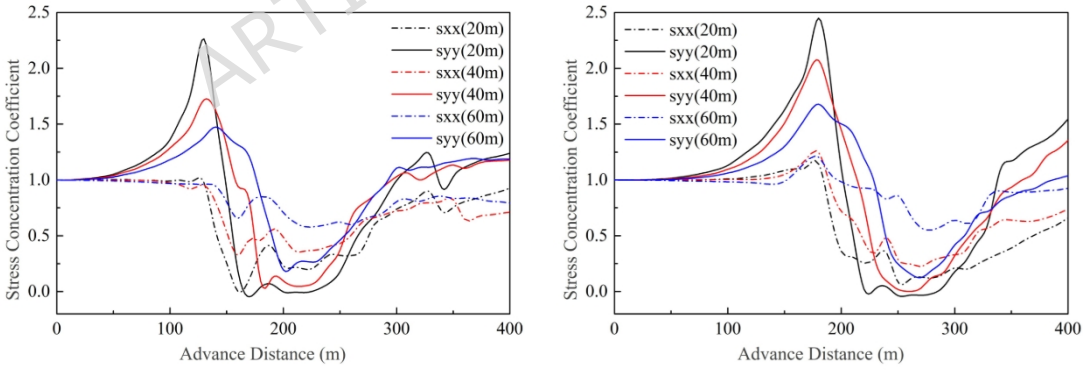

(a) Monitoring Point 150

(b) Monitoring Point 200

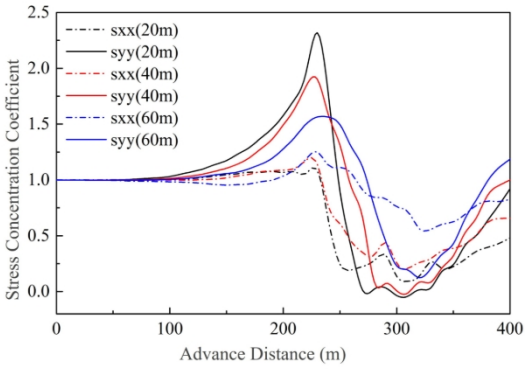

(c) Monitoring Point 250

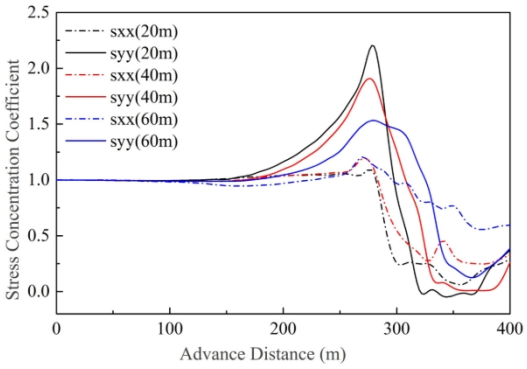

(d) Monitoring Point 300

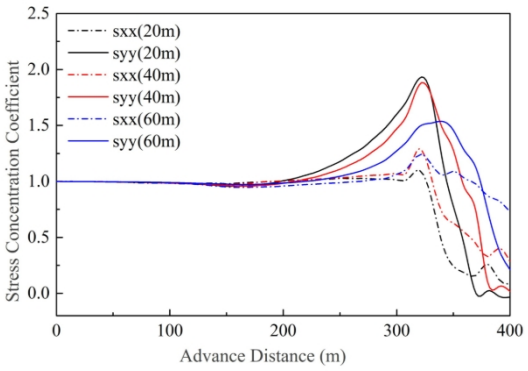

(e) Monitoring Point 350

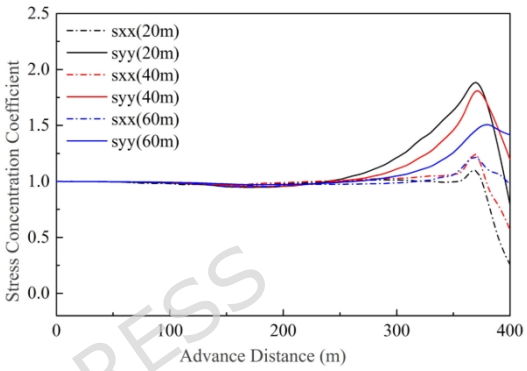

(f) Monitoring Point 400

Fig. 5 Stress evolution at fixed locations in WRKS during mining

Analysis of Fig. 5 reveals:

(1) Prior to mining disturbance, all monitoring points exhibit virgin stress conditions. When the working face advances to approximately 150 m behind a monitoring point (lead distance), vertical stress at the point progressively increases due to front abutment pressure effects, while horizontal stress remains essentially constant until the lead distance reduces to ~50 m, whereupon horizontal stress initiates its ascent. At a lead distance of ~25 m, both vertical and horizontal stresses peak simultaneously. Taking Monitoring Point 200 as an example, at relative interburden thicknesses η=5, 10, and 15, the maximum vertical stress concentration coefficients register 2.44, 2.08, and 1.68 respectively, while maximum horizontal stress concentration coefficients measure 1.18, 1.27, and 1.22 respectively, demonstrating significantly greater stress concentration in the vertical direction than the horizontal.

(2) As the coal seam advance continues, exemplified by Monitoring Point 150, both vertical and horizontal stresses undergo rapid unloading, with minimum stress concentration coefficients at η=5, 10, and 15 registering 0.02, 0.06, and 0.18 for vertical stress, and 0.10, 0.33, and 0.57 for horizontal stress, demonstrating significantly greater unloading magnitude in the vertical direction compared to the horizontal.

(3) Following a period of sustained maximum unloading, both vertical and horizontal stresses gradually recover towards near-virgin stress levels, attaining relative stability. The stress recovery distances for vertical stress at relative interburden thicknesses η=5, 10, and 15 register 152 m, 139 m, and 117 m respectively, while horizontal stress recovery distances measure 187 m, 172 m, and 169 m, indicating faster recovery kinetics in the vertical direction. At 400 m working face advance, vertical stress concentration coefficients reach 1.23 (η=5), 1.17 (η=10), and 1.18 (η=15), demonstrating excess recovery beyond virgin stress conditions. Conversely, horizontal stress concentration coefficients stabilize at 0.92 (η=5), 0.71 (η=10), and 0.79 (η=15), failing to recover to pre-mining levels. This occurs because vertical stress, governed by constant gravitational loading, can be rebuilt through passive compaction of the fractured rock mass. In contrast, horizontal stress relies on the structural integrity of the rock mass, and mining-induced damage significantly reduces the ability of the WRKS to transfer horizontal forces. Such a pronounced stress imbalance—characterized by high vertical stress and low horizontal stress—severely compromises the water-resisting capacity of the WRKS. The insufficient horizontal stress prevents fractures within the stratum from closing under vertical compression, allowing them to remain open or even propagate, thereby forming stable seepage pathways. Concurrently, the shear strength of the rock mass is significantly diminished, making it prone to shear failure under mining-induced disturbances. This can lead to the development of interconnected water-inrush channels, ultimately resulting in the complete loss of the water-

resisting function of the WRKS.

In summary, the generalized stress evolution sequence of the WRKS during mining operations is characterized by four distinct phases: (1) Initial virgin stress equilibrium; (2) Stress escalation to peak magnitudes under front abutment pressure influence as the working face advances; (3) Rapid stress unloading to minimum values upon entering the goaf domain, followed by a sustained relief state; and (4) Gradual stress recovery approximating virgin stress levels through overburden compaction effects, ultimately achieving a quasi-stable stress condition.

During coal extraction, a fixed monitoring point within the WRKS ahead of the working face undergoes a defined stress trajectory: "Virgin stress → Stress concentration → Pressure relief → Sustained relief → Stress recovery → Asymptotically approaching virgin stress." Spatially, the WRKS is subdivided into four distinct stress domains: Virgin stress zone, Stress concentration zone, Pressure relief zone, and Stress recovery zone. Temporally, the WRKS sequentially experiences three evolutionary phases: Stress loading, unloading, and recovery under mining-induced disturbance.

3.2 Spatiotemporal distribution and evolutionary mechanisms of mining-induced fractures in WRKS

The predefined orthogonal joint network (longitudinal and transverse) within the WRKS of the numerical model enables simulation of joint aperture dynamics—dilation or closure—during coal seam extraction and overlying strata movement. These joint responses mechanistically characterize fracture propagation and closure behaviors in the WRKS. Fig. 6 illustrates the spatial distribution of dilated joints within the WRKS at working face advance distances of 150, 200, 250, 300, 350, and 400 m under varying interburden thickness conditions, providing direct visualization of mining-induced fracture networks.

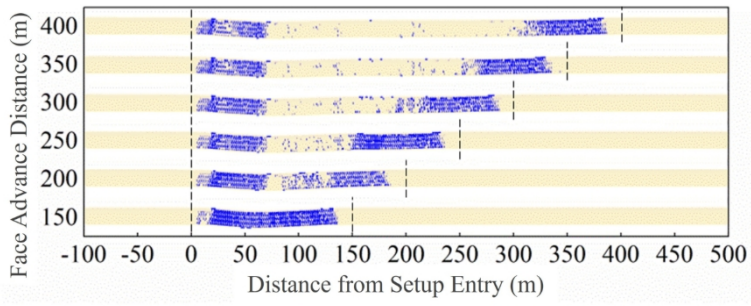

(a) Relative interburden thickness η=5

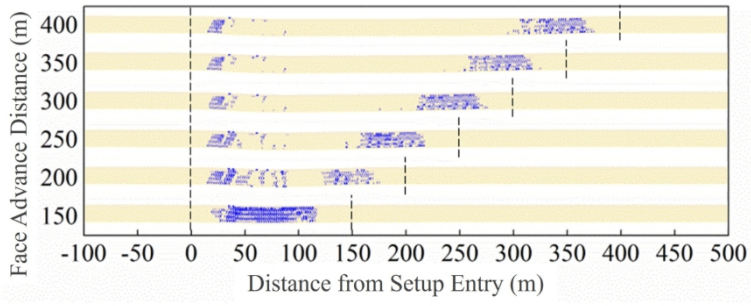

(b) Relative interburden thickness η=10

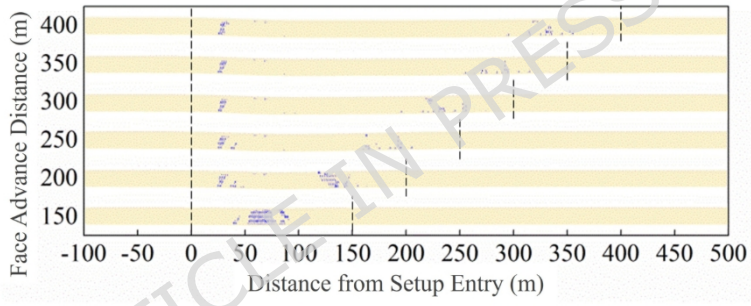

(c) Relative interburden thickness η=15

Fig.6 Spatial distribution of fractures in WRKS during mining

Analysis of Fig. 6(a) demonstrates:

(1) At 150 m advance, extensive fracture development occurs within the WRKS overlying the goaf area; by 200 m advance, fractures in the central goaf initiate closure, forming a distinct closed fracture zone. As mining progresses, persistent fracture development zones with stable dimensions (65 m ahead of the setup entry and 72 m behind the working face) are maintained, while the closed fracture zone expands progressively—measuring 0 m at 150 m advance, 57 m (200 m), 78 m (250 m), 143 m (300 m), 196 m (350 m), and 240 m (400 m).

(2) At a fixed advance distance of 300 m, fracture development zones ahead of the setup entry measure 65 m, 24 m, and 7 m for relative interburden thicknesses η=5, 10, and 15 respectively, while

zones behind the working face span 72 m, 60 m, and 37 m. This progressive contraction of fracture development extent with increasing η results from attenuated mining disturbance effects on the WRKS under identical geomechanical conditions, whereby greater vertical separation reduces strata deformation magnitude and kinematic energy transfer.

(3) During mining operations, the fracture development zone ahead of the setup entry remains spatially fixed, while the zone behind the working face migrates synchronously with face advance. Comparative analysis of Fig. 6(a) and Fig. 2(a) reveals that fracture development zones exhibit a high degree of spatial correspondence with pressure relief zones, demonstrating a strong mechanistic coupling between mining-induced fracture propagation and stress redistribution within the WRKS, as evidenced in Fig. 7.

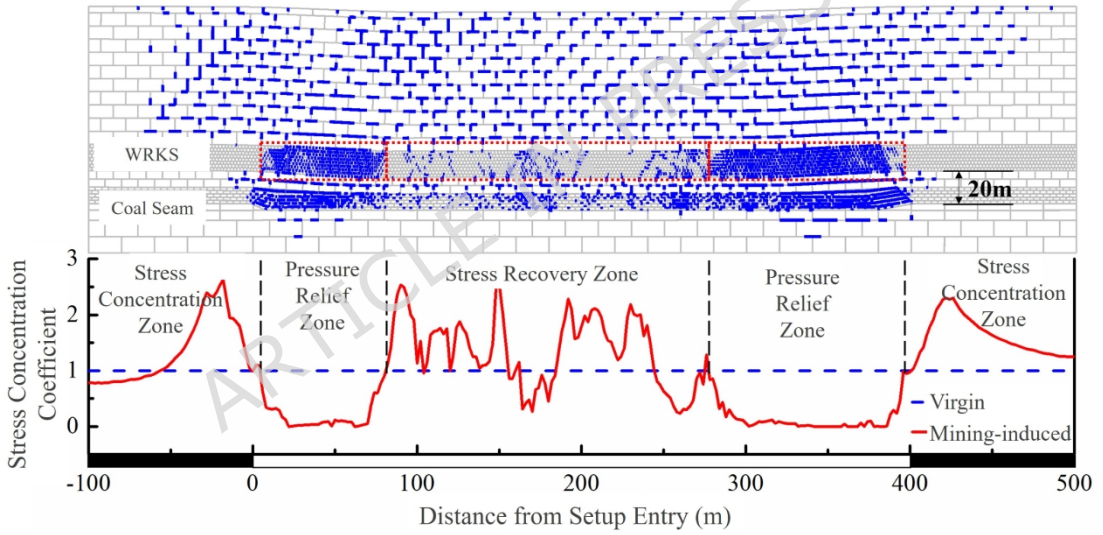

Fig.7 Coupling between fracture development and mining-induced stresses in WRKS: exemplified by relative interburden thickness η=5

To investigate the propagation and closure dynamics of mining-induced fractures within the WRKS, six monitoring sectors were established at the following locations: 90-110 m, 140-160 m, 190-210 m, 240-260 m, 290-310 m, and 340-360 m ahead of the setup entry. Fracture ratio—defined as the proportion of dilated joint length to total joint length within each sector—was quantified and plotted against working face advance distance, with the resulting temporal evolution curves presented in Fig. 8.

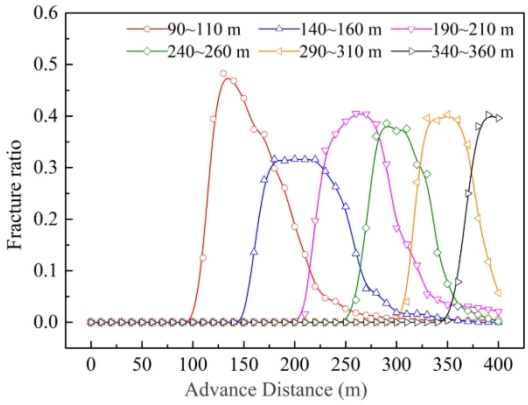

(a) Relative interburden thickness η=5

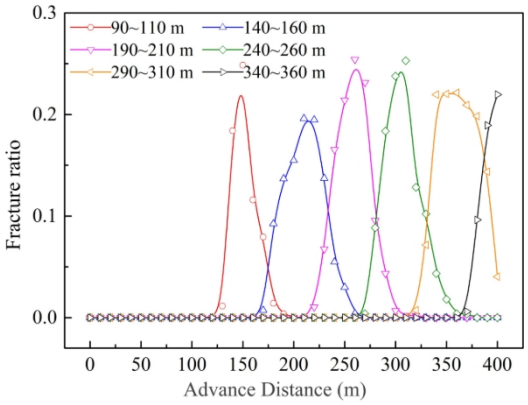

(b) Relative interburden thickness η=10

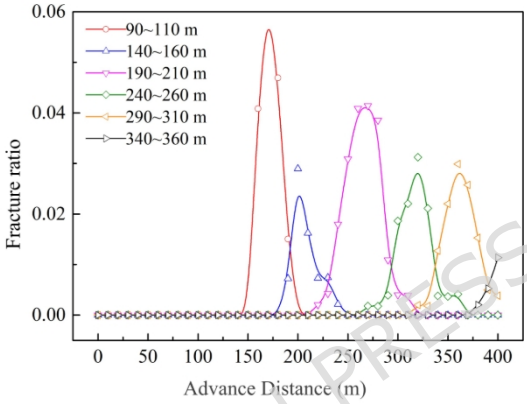

(c) Relative interburden thickness η=15

Fig. 8 Temporal evolution curves of fracture ratio across designated monitoring sectors in the WRKS

Analysis of Fig. 8 reveals that:

(1) Fracture ratios within all monitoring sectors of the WRKS undergo sequential propagation followed by progressive closure during coal seam advance, exemplified at η=5 in the 90-110 m sector: null fracture ratio persists until 94 m advance; ascends to its peak (0.47) during 94-134 m advance; progressively declines to 0.02 over 134-259 m advance; and stabilizes at residual levels from 259-400 m advance.

(2) Exemplified in the 90-110 m monitoring sector, peak fracture ratios at relative interburden thicknesses η=5, 10, and 15 register 0.47, 0.22, and 0.06 respectively, demonstrating progressive attenuation; the advance distance intervals between fracture initiation and quasi-closure states measure 165 m, 77 m, and 64 m respectively, indicating progressively shorter fracture activity durations. These patterns conform to the geomechanical principle

whereby greater vertical distance from the coal seam reduces mining disturbance intensity on the WRKS, resulting in diminished fracture development magnitude and accelerated closure kinetics—consistent with the preceding findings.

3.3 Mining-induced stress paths, fracture evolution characteristics, and their mechanistic coupling in WRKS

Previous research established a strong correlation between fracture dilation/closure characteristics and mining-induced stress variations in the WRKS. Consequently, an integrated analysis of WRKS stress evolution curves and fracture ratio evolution curves was conducted to elucidate their mechanistic interdependence. Fig. 9 presents the synchronized stress trajectory at Monitoring Point 200 and the fracture ratio evolution in Sector 190-210 m during coal extraction.

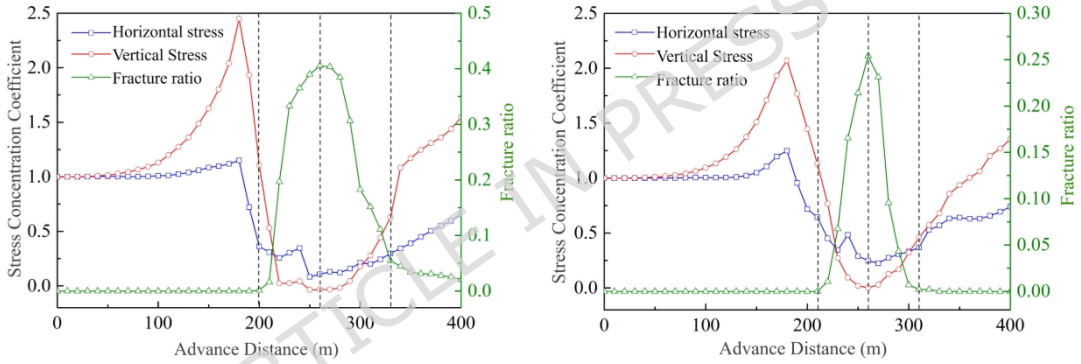

(a) Relative interburden thickness η=5 (b) Relative interburden thickness η=10

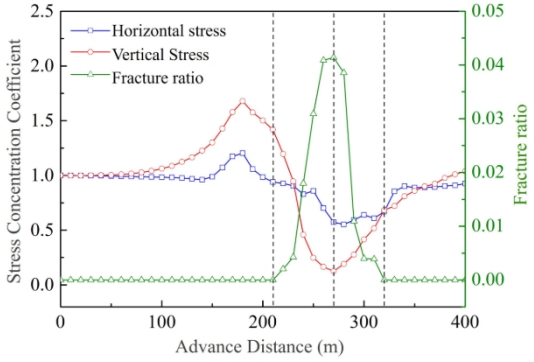

(c) Relative interburden thickness η=15

Fig. 9 Stress paths and fracture ratio evolution curves of the WRKS

Stress-fracture ratio relationship curves for the WRKS exhibit consistent patterns across varying relative interburden thicknesses (η), as exemplified by Fig. 9(a):

(1) During coal seam advancement: From 0-40 m, the WRKS maintains original rock stress equilibrium with no mining-induced fractures; 40-180 m sees vertical stress concentration peak at 2.48 times virgin stress and horizontal at 1.16 times, suppressing fractures through compressive densification; 180-200 m experiences initial unloading reducing vertical stress to 1.12 times and horizontal to 0.36 times original levels without fracture development; 200-260 m exhibits continued unloading where vertical stress drops to 0 times and horizontal to 0.11 times, triggering fracture propagation until reaching maximum fracture ratio 0.40; 260-330 m shows stress recovery increasing vertical stress to 0.64 times and horizontal to 0.30 times original values, closing fractures to ratio 0.06; 330-400 m demonstrates further stress elevation to 1.56 times (vertical) and 0.67 times (horizontal) original stresses, reducing fracture ratio to 0.02 through sustained closure.

(2) At 200 m working face advance, the fracture ratio within the WRKS initiates its ascent coinciding with the unloading phase of vertical and horizontal stresses, indicating decompression failure and fracture initiation in the rock layer. As mining progresses, continued stress reduction correlates with persistent fracture ratio increase, demonstrating that greater pressure relief intensifies fracture development. When stress recovery commences due to overburden compaction, the fracture ratio progressively declines until fractures approach complete closure, establishing a significant inverse correlation between stress magnitude and fracture ratio evolution in the WRKS.

Based on preceding findings, the mining-induced stress path of the WRKS is categorized into six distinct phases: "Virgin Stress → Stress Increase → Pressure Relief → Sustained Pressure Relief → Stress Recovery → Asymptotically Approaching Virgin Stress." Concurrently, the fracture aperture evolution process divides into five stages: "Incubation → Propagation → Stabilization → Closure → Asymptotically Approaching Complete Closure," as schematically illustrated in Fig. 10.

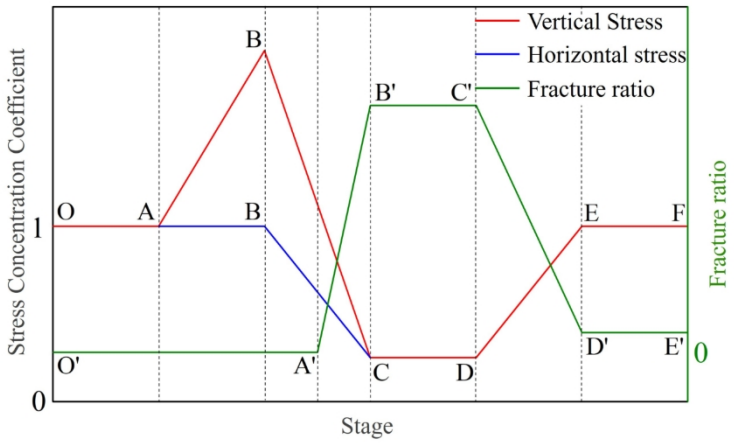

Fig. 10 Mining-induced stress paths and fracture evolution characteristics of WRKS

The mining-induced stress path of the WRKS progresses through six defined stages: (1) OA (Virgin Stress): Unaffected by mining, maintaining hydrostatic in-situ stress; (2) AB (Stress Increase): Vertical stress rises to the front abutment peak while horizontal stress remains near-constant; (3) BC (Pressure Relief): Substantial reduction in both vertical/horizontal stresses upon goaf entry; (4) CD (Sustained Relief): Full pressure relief under goaf and coal wall support; (5) DE (Stress Recovery): Progressive stress increase via goaf compaction; (6) EF (Asymptotically Approaching Virgin Stress): Stress nears pre-mining equilibrium under sustained compaction.

Correspondingly, WRKS fracture evolution follows five phases: (1) O´A´ (Incubation): Pre-existing fractures compact during stress increase, with dilation tendency initiating in early relief; (2) A´B´ (Propagation): Rapid fracture development during stress unloading; (3) B´C´ (Stabilization): Peak fracture density under sustained pressure relief; (4) C´D´ (Closure): Progressive fracture sealing during stress recovery; (5) D´E´ (Asymptotically Approaching Complete Closure): Residual fractures persist at minimal aperture without complete sealing.

4 Conclusions

The core innovation of this research is the establishment of a dynamic stress-fracture evolution sequence of the WRKS above the working face as a function of the relative interburden thickness throughout the entire mining process. The principal conclusions are

as follows:

(1) During the initial mining stage after the first weighting of the main roof but before central goaf compaction, the spatial stress distribution within the overlying WRKS follows the sequence: Initial Stress Zone - Stress Concentration Zone - Pressure Relief Zone - Stress Concentration Zone - Initial Stress Zone. Following the onset of central goaf compaction, this configuration transitions to: Initial Stress Zone - Stress Concentration Zone - Pressure Relief Zone - Stress Recovery Zone - Pressure Relief Zone - Stress Concentration Zone - Initial Stress Zone.

(2) The WRKS exhibits progressively attenuated mining disturbance effects with increasing relative interburden thickness (η), characterized by reduced stress variation amplitudes: the maximum stress concentration coefficient within stress concentration zones declines systematically, while the minimum stress concentration coefficient in pressure relief zones rises; as η asymptotically approaches infinity, mining disturbance diminishes to negligible levels, resulting in the WRKS persistently maintaining virgin stress equilibrium unaffected by extraction activities.

(3) The fracture development zone within the WRKS exhibits a high degree of spatial coincidence with the pressure relief zone, demonstrating a strong mechanistic coupling between fracture propagation and mining-induced stress redistribution. Furthermore, the spatial extent, duration, and fracture density of the fracture development zone all exhibit negative correlations with the relative interburden thickness under equivalent geomechanical conditions.

(4) The mining-induced stress path of the WRKS progresses through six defined phases: Virgin Stress → Stress Increase → Pressure Relief → Sustained Pressure Relief → Stress Recovery → Asymptotically Approaching Virgin Stress. Concurrently, the evolution of mining-induced fractures follows five distinct stages: Incubation → Propagation → Stabilization → Closure → Asymptotically Approaching Complete Closure.

The findings of this study provide practical engineering guidance

for water conservation and hazard prevention in mining operations. The core approach involves obtaining the parameter of "relative interburden thickness" through pre-mining geological exploration to enable rapid preliminary assessment of WRKS stability: ① When the relative interburden thickness is small (e.g., ≤5 as in the presented case), the WRKS lies within the caved zone where its structure undergoes complete failure after mining, losing water-resisting capacity. This necessitates proactive measures such as pre-drainage; ② With moderate relative interburden thickness (e.g., =10), the WRKS located in the fractured zone exhibits dynamic stability during mining, requiring optimized panel layout and controlled mining rates to suppress excessive fracture development; ③ When the relative interburden thickness is large (e.g., ≥15), the WRKS positioned in the continuous deformation zone maintains structural integrity post-mining, serving as an ideal natural water-resisting barrier that should be prioritized for protection in mining design. For mining operations conducted under aquifers with unfavorable geological conditions, such as those with thin bedrock (which typically results in a small η value), the guidance provided by this study is particularly significant. When a diagnostically small η value is identified, the engineering focus must decisively shift to proactive drainage and robust support. When the η value falls within a moderate range, efforts should be directed towards controlling mining parameters and exploring artificial reinforcement techniques (e.g., grouting) to utilize the stress recovery phase for fracture closure. Therefore, even when geological conditions pose constraints, the established relationship between η and the stress-fracture evolution offers a critical decision-making basis for selecting the most appropriate and safe mining method.

The numerical model developed in this study and the resulting conclusions are primarily applicable to idealized geological conditions involving nearly horizontal coal seams and relatively homogeneous lithological combinations. For inclined coal seams, their asymmetric stress distribution and fracture patterns may

significantly alter the mining-induced stress and fracture evolution characteristics of the WRKS. Consequently, the control law of relative interburden thickness revealed in this study requires modification under such conditions. Similarly, in complex strata with frequent lithological variations and developed weak interlayers, the mechanical interactions between rock layers become more intricate. These weak interlayers may alter the vertical propagation pathways of fractures and the efficiency of stress transfer. Therefore, direct extrapolation of the quantitative findings of this study to such complex conditions must be exercised with great caution.

On the other hand, the findings and mechanistic insights presented in this study are derived from numerical simulations under idealized conditions. While this approach was instrumental in clarifying the controlling effect of relative interburden thickness on the WRKS, future research should aim to validate the conclusions through data obtained from physical simulations and in-situ field monitoring. Validating these findings under more complex geological conditions will be a critical step toward developing universally applicable strategies for water conservation in mining.

CRediT authorship contribution statement

Huadong Gao: Writing – original draft, Visualization, Validation, Methodology, Investigation, Formal analysis, Data curation, Conceptualization. **Li Ji:** Writing – review & editing, Validation, Supervision, Methodology, Conceptualization. **Yanli Huang:** Writing – review & editing, Funding acquisition. **Junmeng Li:** Writing – review & editing, Funding acquisition.

Declaration of Competing Interest

The authors declare that they have no known competing financial interests or personal relationships that could have appeared to influence the work reported in this paper.

Data availability

The datasets generated and/or analysed during the current study are not publicly available due to confidentiality requirements but are

available from the corresponding author on reasonable request.

Funding

Financial support of this work is provided by the National Natural Science Foundation of China (Grant number: 52022107, 52174128 and 52374245).

References:

1. Fan, L., Sun, Q., Ma, L., Li, T. & Chen, H. Technological system of water-conserving coal mining. *Coal Geology and Exploration*. **51**, 196-204 (2023).
2. Fan, L. Geological technological innovations and contributions in the exploration and development of the Shenfu coalfield. *Coal Geology and Exploration*. **53**, 1-22 (2025).
3. Wang, S., Wei, J., Song, S., Wang, S. & Sun, T. Influence of thick sandstone on development of overburden mining fissures in northern Shaanxi coal mining area of yellow river basin and suggestions on water-preserved coal mining. *Coal Geology and Exploration*. **50**, 1-11 (2022).
4. Huang, Y. et al. Ecological and environmental damage assessment of water resources protection mining in the mining area of western China. *Ecol. Indic.* **139**, 108938 (2022).
5. Liu, C. et al. Law of overburden failure and mechanism of water inrush and support crushing in extra-thick coal seam mining within an anticline structural area. *Journal of Mining and Safety Engineering*. **42**, 239-251 (2025).
6. Liao, X. & Qian, M. Research on green mining of coal resources in China: Current status and future prospects. *Journal of Mining and Safety Engineering*. **26**, 1-14 (2009).
7. Zhao, C. et al. Analysis on water loss characteristics of roof aquifer and borehole hydraulic curtain protection in deep coal mining in inner Mongolia-Shaanxi mining area. *Coal Geology and Exploration*. **51**, 88-98 (2023).
8. Li, Q., Meng, X. & Liu, Y. Sensitivity analysis of water inrush evaluation model based on the theory of water resistant key strata: A case study in a coal mine, China. *Earth Sci. Inform.* **15**, 2481-2494 (2022).
9. Guo, J. & Ma, L. Permeability distribution characteristics and water resistance evaluation of interlayer rock strata during multi-seam coal mining. *Mine Water Environ.* **44**, 239-258 (2025).
10. Sun, Q., Jiang, Y., Ma, D., Zhang, J. & Huang, Y. Mechanical model and engineering measurement analysis of structural stability of key aquiclude strata. *Mining Metallurgy and Exploration*. **39**, 2025-2035 (2022).
11. Zhou, H. W. et al. Creep-based permeability evolution in deep coal under unloading confining pressure. *J. Nat. Gas Sci. Eng.* **65**, 185-196 (2016).
12. Wang, Z., Li, W. & Hu, Y. Experimental study on mechanical behavior, permeability, and damage characteristics of jurassic sandstone under varying stress paths. *Bull. Eng. Geol. Environ.* **80**, 4423-4439 (2021).

13. Kang, H. & Gao, F. Evolution of mining-induced stress and strata control in underground coal mines. *Chinese Journal of Rock Mechanics and Engineering*. **43**, 1-40 (2024).
14. Deng, D., Wang, H., Xie, L., Wang, Z. & Song, J. Experimental study on the interrelation of multiple mechanical parameters in overburden rock caving process during coal mining in longwall panel. *International Journal of Coal Science and Technology*. **10**, 47 (2023).
15. Huang, M., Zhang, L., Zhang, C. & Chen, S. Characteristics of permeability changes in bituminous coal under conditions of stress variation due to repeated mining activities. *Nat. Resour. Res.* **29**, 1687-1704 (2020).
16. Xie, H. et al. Stress-fracture-seepage field behavior of coal under different mining layouts. *Journal of China Coal Society*. **41**, 2405-2417 (2016).
17. Cui, F. et al. Study on advancing rate of steeply inclined extra-thick coal seam in rock burst mine based on loading-unloading response ratio. *Journal of China Coal Society*. **47**, 745-761 (2022).
18. Gao, M. et al. In-situ disturbed mechanical behavior of deep coal rock. *Journal of China Coal Society*. **45**, 2691-2703 (2020).
19. Zhang, L., Kan, Z., Xue, J., Li, M. & Zhang, C. Study on permeability law of intact and fractured coals under cyclic loading and unloading. *Chinese Journal of Rock Mechanics and Engineering*. **40**, 2487-2499 (2021).
20. Ma, K. et al. Mechanical model for analyzing the water-resisting key stratum to evaluate water inrush from goaf in roof. *Geomech. Eng.* **28**, 299-311 (2022).
21. Chai, J. et al. Pressure relief effect of protective layer mining and its optical fiber monitoring. *Journal of China Coal Society*. **47**, 2896-2906 (2022).
22. Xie, P., Huang, B., Wu, Y., Chen, J. & Liu, W. Time-space effect of overburden stress path in steeply dipping and large mining height stope. *Journal of China Coal Society*. **48**, 424-436 (2023).
23. Pang, Y., Wang, G. & Li, B. Stress path effect and instability process analysis of overlying strata in deep stopes. *Chinese Journal of Rock Mechanics and Engineering*. **39**, 682-694 (2020).
24. Wang, L. et al. Failure analysis of rock strata between upper and lower coals under underground reservoir in coal mine and its critical percolation model of jumping permeability. *Journal of China Coal Society*. **48**, 1192-1208 (2023).
25. Ran, Q. et al. Characteristics of mining-induced fractures under inclined coal seam group multiple mining and implications for gas migration. *Nat. Resour. Res.* **32**, 1481-1501 (2023).
26. Zhao, P. et al. Research on the evolution mechanism of the topological relationship of the property parameters of the mining overburden rock pressure relief gas migration channel. *Coal Science and Technology*. **52**, 135-149 (2024).
27. Wu, B. et al. Influence of high salt mine water storaged in underground reservoir of coal mine on groundwater. *Journal of China Coal Society*. **46**, 2360-2369 (2021).
28. Liang, T., Liu, X. & Wang, S. Fractal study on the crack network evolution and

permeability change in mining rock mass. *Journal of China Coal Society*. **44**, 3729-3739 (2019).
29. Yin, G. et al. Experimental study on overburden strata fracture evolution law in three dimensional mine-induced stress conditions. *Journal of China Coal Society*. **41**, 406-413 (2016).
30. Zhang, B., Sun, H., Liang, Y., Wang, K. & Zou, Q. Characterization and quantification of mining-induced fractures in overlying strata: implications for coalbed methane drainage. *Nat. Resour. Res.* **29**, 2467-2480 (2020).
31. Liu, J. et al. Study on fractal characteristics of fracture network in overlying strata mining under different breaking distances. *Journal of Shandong University of Science and Technology (Natural Science)*. **43**, 11-21 (2024).
32. Chen, K., Ge, Y., Zhang, Q., Chen, L. & Liu, Z. Discrete element simulation for crack fractal evolution laws associated with slicing mining in super thick coal stratum. *Journal of Engineering Geology*. **29**, 1113-1120 (2021).
33. Zhuo, H., Qin, B., Shi, Q. & Li, L. Development law of air leakage fractures in shallow coal seams: A case study in the Shendong coalfield of China. *Environ. Earth Sci.* **77**, 772 (2018).
34. Chen, J. et al. An experimental and analytical research on the evolution of mining cracks in deep floor rock mass. *Pure Appl. Geophys.* **177**, 5325-5348 (2020).
35. Yao, W., Wang, E., Liu, X. & Zhou, R. Fracture distribution in overburden strata induced by underground mining. *Deep Underground Science and Engineering*. **1**, 58-64 (2022).
36. Ma, J. et al. The study on the propagation laws of hydraulic fractures in coal measure strata under true triaxial conditions. *Journal of Mining and Strata Control Engineering*. 7, 1-24 (2025).
37. Liu, Y. et al. Acoustic-thermal response characteristics and precursor law of fractured sandstone under cyclic loading and unloading. *Rock Soil Mech.* **46**, 1-19 (2025).
38. Li, X. & Huang, Q. High development characteristics of water flowing fractured zone in fully-mechanized top-caving mining of extremely thick coal seam under water. *Journal of Mining and Safety Engineering*. **39**, 54-61 (2022).
39. Li, T. Evolutionary pattern of pressure-relief gas transportation-storage area in fully mechanized mining face and its engineering practice in Huangling minefield. *Journal of China Coal Society*. **49**, 995-1006 (2024).
40. Sun, Q., Liu, H., Zhang, J., Zhou, N. & Ma, D. Mechanical model and analysis of seepage stability in key aquiclude strata during backfill mining. *Journal of Mining and Safety Engineering*. **39**, 273-281 (2022).
41. Xu, Z. et al. Simulation experiment on the structural evolution and damage-deterioration mechanism of boundary coal pillars under immersion in abandoned mines. *Journal of China Coal Society*. **50**, 1100-1114 (2025).
42. Huang, G. Discussion on the practical application of hydrogeological and engineering geological survey standards in mining areas. *Nonferrous Metals Design*. **52**, 21-26 (2025).

43. Lv, Y., Sun, G., Wu, B. & Li, S. Discussion on safety of coal (rock) pillar in "three down" mining standards. *Coal Science and Technology*. **52**, 139-145 (2024).
44. Zheng, K. et al. Calculation method and evolution mechanism of surrounding rock energy during excavation unloading of deep tunnels in high in-situ stress field. *Rock Soil Mech.* **46**, 165-177 (2025).
45. Zuo, J. et al. True triaxial failure behavior and structure-material synergistic failure mechanism of coal-rock composites. *Journal of China University of Mining and Technology*. **54**, 287-303 (2025).
46. Zhang, P. *Study on soil damage caused by crack development in shallow coal mining in loess sand-blown region*. Xuzhou: China University of Mining and Technology, 2022.
47. Sun, Q. *Mechanism and method of key aquiclude strata reconstruction by backfill mining technology*: China University of Mining and Technology, 2019.